ISSN 0030-400X, Optics and Spectroscopy, 2015, Vol. 119, No. 2, pp. 171–186. © Pleiades Publishing, Ltd., 2015.
Original Russian Text © A.P. Chaynikov, A.G. Kochur, V.A. Yavna, 2015, published in Optika i Spektroskopiya, 2015, Vol. 119, No. 2, pp. 179–194.

SPECTROSCOPY OF ATOMS AND MOLECULES

Charge, Photon, and Electron Spectra upon Cascade Decay of the States of the Neon Atom that Arise As a Result of Photoionization Near the *K*-threshold

A. P. Chaynikov, A. G. Kochur, and V. A. Yavna

Rostov State Transport University, Rostov-on-Don, 344038 Russia

e-mail: chaynikov.a.p@gmail.com

Received February 18, 2015; in final form, March 19, 2015

Abstract—We have calculated emission spectra of photons and electrons and charge spectra of final ions which are produced by the cascade decay of states created by photoionization of the neon atom near the *K*-threshold. Calculations have been performed by straightforward construction of cascade decay trees. Branching probabilities have been calculated in the Pauli–Fock single-configuration approximation. We have taken into consideration additional monopole excitations and ejections which accompany the 1*s*-photoionization process as well as the radiative and nonradiative transitions in the course of cascade. As the energy of excitation photons increases, the spectra of cascade photons and electrons acquire a more and more complicated satellite structure, with the probability of formation of final ions with a higher charges increasing.

DOI: 10.1134/S0030400X15080056

INTRODUCTION

Creation of a vacancy in an inner electron shell of an atom, e.g., as a result of photoabsorption, transfers the atom into a strongly excited unstable state, which is subjected to decay. A vacancy can decay either radiatively or nonradiatively (Auger, Coster–Kronig, and super-Coster–Kronig processes). Radiative transitions are accompanied by emission of a photon and lead to the transfer of the vacancy to a higher-lying electron shell. Upon nonradiative transitions, the initial vacancy is filled, and electron ejection and formation of two new vacancies in higher-lying shells take place. At the first step of the decay, the initial excited state with a vacancy in an inner shell decays as a result of radiative and/or nonradiative transitions into a set of states with vacancies in higher-lying shells. In turn, these states can decay further if there are electrons in higher outer shells. Calculations and experiments show that transitions with the participation of shells nearest to a shell with a decaying vacancy are, as a rule, most probable. In connection with this, the decay of an inner vacancy in many-electron atoms is a complex multistep cascade process, which consists of successive radiative and nonradiative transitions and which proceeds until, as a result of some later step, all vacancies are transferred to outermost shells. The ejection of electrons upon nonradiative transitions in an atom leads to its multiple ionization [1–3]. Since radiative and nonradiative transitions occur from a large number of various hole configurations that arise as the cascade decay proceeds, photon emission spectra and electron spectra have complex multicomponent structures [4–7].

A sudden change of the potential of the atomic core during the creation of an inner vacancy may lead to an additional monopole excitation or ionization of electrons of outer shells into the states with the same orbital quantum numbers [8–11]. In the English-language literature, these processes are referred to as "shake processes." One distinguishes between shake-up (SU) processes, as a result of which an outer electron is excited to a bound state of a discrete spectrum, and shake-off (SO) processes, due to which an electron is ejected into states of the continuous spectrum.

In emission spectra of photons [12] and electron spectra [13, 14] created by the cascade decay of an inner vacancy, the shake processes give rise to the appearance of different satellite structures. In the charge spectra of ion yields, shake processes contribute to the formation of ions with charges that are higher than those that are expected upon consideration only of diagram transitions from states without additional excitations [15, 16]. In X-ray absorption spectra, opening of channels of additional excitation/ionization above the ionization threshold of an inner shell disturbs the smoothness of the atomic photoabsorption cross section [17–19].

Because various SU and SO processes can occur at different energies (different opening energies of channels), there is the possibility to trace corresponding changes in electron, photon, and charge spectra created by the cascade decay of the inner vacancy upon

variation of the energy of photons or ionizing particles. This has been shown, e.g., in ref. [20], which was devoted to the theoretical simulation of cascade decay processes in gaseous boron that were caused by the photoionization of the 1*s* shell and in which changes in cascade spectra upon variation in the energy of incident photons were studied.

It should be noted that electrons and photons emitted by an ionized atom, especially at first steps of the cascade decay, may have energies sufficient to ionize neighboring atoms. One should consider these processes in the theoretical description of the effect of ionizing radiations on various compounds and biological objects. Therefore, obtaining information on spectra of photons and electrons created by cascade decays is an important problem.

This work is devoted to theoretical investigation of the cascade decay of a 1*s* vacancy in the neon atom that arises as a result of its photoionization at energies of an absorbed photon that correspond to opening of different channels of additional SU and SO processes that accompany the 1*s*-ionization. We have studied this problem in [21], in which we restricted ourselves to taking into account SU excitations of 2*s*/2*p* electrons only to nearest 3*s*/3*p* states. In this work, we increase the number of SU-processes to be taken into account and consider additional excitations into (4*s*, 5*s*)/(4*p*, 5*p*) subshells and consider SO processes that accompany intraatomic radiative and nonradiative transitions.

The basic objective of this work is to show how various SU and SO processes that accompany the photoionization of an inner shell affect the photon emission, Auger electron emission, and ion-yield spectra that arise as a result of the cascade decay of states created by the photoionization.

METHOD OF CALCULATION

The method of calculation of characteristics of the cascade decay of an inner vacancy that is used in this work is based on a straightforward construction of the decay tree [15, 16]. Below, we present its brief description.

Let $C^{(0)}$ be the electron configuration of an initial ion with one or several vacancies. At the first step of the cascade decay, the configuration $C^{(0)}$ decays into states with configurations $C_1^{(1)}$, $C_2^{(1)}$, ..., $C_n^{(1)}$, which form a set of configurations of the first generation, $\{C_k^{(1)}\}$. At the second step of the decay, configurations from set $\{C_k^{(1)}\}$ decay further and, taking into account all possible decay channels for each configuration $C_k^{(1)}$, a set of configurations of the second generation is formed, $\{C_k^{(2)}\}$. This process proceeds until a set of configurations is formed after some ensuing step of the decay that is such that none of its configurations may decay further.

The initial $C^{(0)}$ and all intermediate configurations $C_k^{(i)}$ form branching points of the decay tree. All energetically allowed radiative and nonradiative transitions $C_k^{(i)} - C_m^{(i+1)}$ are branches of the decay tree and originate from branching point $C_k^{(i)}$. Each branch of the decay tree is characterized by a ratio (probability) of branching,

$$\chi(C_k^{(i)} - C_m^{(i+1)}) = \frac{\Gamma(C_k^{(i)} - C_m^{(i+1)})}{\sum_{m'} \Gamma(C_k^{(i)} - C_{m'}^{(i+1)})}, \quad (1)$$

where $\Gamma(C_k^{(i)} - C_m^{(i+1)})$ is the partial width of state $C_k^{(i)}$ due to the $C_k^{(i)} - C_m^{(i+1)}$ transition, while the sum over all $C_{m'}^{(i)}$ configurations is the total width of state $C_k^{(i)}$.

In this work, partial widths of radiative and nonradiative transitions are calculated using approximations in terms of which it is possible to represent the widths of transitions in the form of a product of two factors, one of which depends only on occupation numbers, while the other depends on radial parts of wave functions of electrons that participate in the transition [15, 16].

Partial widths of radiative transitions are calculated by the formula (here and below, the atomic system of units is used, while upper indices that indicate the number of the decay step are omitted)

$$\Gamma_{i-j}(C_k - C_m) = N_i^{\nu} N_j \frac{4}{3}\left(\frac{E_{ij}}{c}\right)^3 \frac{\max(l_i, l_j)}{2(2l_i+1)(2l_j+1)} R_{ij}^2. \quad (2)$$

In this formula, the indices i and j denote the shells with initial and final vacancies, respectively, that are involved in the transition; N_i^{ν} is the number of vacancies, while N_j is the number of electrons in corresponding shells prior to the transition; E_{ij} is the transition energy; c is the speed of light; l_i, l_j are the orbital quantum numbers; and R_{ij} is the radial part of the matrix element of the dipole transition operator

$$R_{ij} = \langle n_i l_i | r | n_j l_j \rangle. \quad (3)$$

Partial widths of nonradiative transitions are calculated by the formula

$$\Gamma_{i-jk}(C_k - C_m) = N_i^{\nu} N_{jk} \gamma_{ijk}. \quad (4)$$

Here, N_i^v has the same meaning as in (2), while N_{jk} is the number of ways to extract a pair of electrons from shells j and k,

$$N_{jk} = \begin{cases} N_j N_k, & j \neq k, \\ N_j(N_j - 1)/2, & j = k. \end{cases}$$

Quantity γ_{ijk} is the so-called partial width per pair of electrons [22], which is a combination of Slater integrals $R^q(n_i l_i \varepsilon l; n_j l_j n_k l_k)$, where εl is the radial part of the wave function of the Auger electron.

It follows from calculations of [15, 16] that matrix elements of the dipole transition operator R_{ij} and partial widths per pair of electrons γ_{ijk} depend almost linearly on the number of vacancies in the shells of a decaying ion, with the contributions to changes of these quantities related to the occurrence of vacancies in different shells being additive. This makes it possible to use interpolation and to rather easily take into account the dependences of R_{ij} and γ_{ijk} on the configuration of the ion [23].

States of a decaying ion at intermediate steps of the cascade development have, as a rule, a complex multiplet structure, which is related to the electrostatic and spin–orbit interactions of electrons of unfilled shells. For this reason, cascade spectra of photons and electrons may contain a large number of multiplet components. In this work, we neglect the multiplet splitting; therefore, each $C_k - C_m$ transition is represented in the spectrum by only one line. Of course, this considerably simplifies spectra, but still makes it possible to examine basic features of their dependence on the energy of the absorbed photon.

In order to calculate matrix elements (3) and partial widths per pair of electrons (4), we used the Hartree–Fock–Pauli approximation with averaging over the configuration [24]. Upon the radiative transition, the radial parts of atomic orbitals i and j are optimized in the configuration of the initial state with vacancy i^{-1}. Upon the nonradiative transition, atomic orbitals i, j, and k were obtained in the configuration with initial vacancy i^{-1}, while the wave functions of Auger electrons are optimized in the $j^{-1}k^{-1}$ core potential built on orbitals of configuration i^{-1}. This approximation is justified by the fact that, upon using orbitals of the initial state of the transition, outer orbitals j and k, which are most sensitive to a change of the potential, are obtained in the correct potential, whereas orbital i of the initial vacancy is less sensitive to a change of the potential.

A change in the potential of the atomic core upon diagram radiative or nonradiative transition $C_k - C_m$, as well as upon photoionization, may lead to SU or SO processes. This gives rise to additional branching of each of the branches corresponding to the diagram transition. In this case, branching ratios are determined via probabilities of shake processes.

In this work, in order to calculate probabilities of shake processes, we used the approximation of sudden perturbations (see, e.g., [25]). The first calculations in terms of this approximation were performed by Migdal [26] and Feinberg [27] as early as in the 1940s for shake processes caused by β-decay of the nucleus. However, the authors of these works used hydrogen-like wave functions, which significantly restricted the potential of the method and the calculation accuracy. First calculations with the use of Hartree–Fock wave functions, which became possible with the development of computation hardware, were performed by Sachenko and Demekhin [8], and by Carlson and Nestor [28].

In sudden approximation, the total probability of the SU and SO processes of excitation/ejection of an additional electron from the nl subshell that are caused by the $C_k - C_m$ transition is determined by the relation

$$w_{\mathrm{SU+SO}}(C_k - C_m, nl) = kN_{nl}(1 - \langle nl[C_k] | nl[C_m] \rangle^2). \quad (5)$$

Here, N_{nl} is the occupation number of the nl subshell in initial configuration C_k, while $\langle nl[C_k] | nl[C_m] \rangle$ is the overlap integral of orbitals nl, which are optimized in configurations C_k and C_m.

Upon taking into account the shake processes which accompany diagram transitions, in this work, we used an approximation in terms of which the probability (5) refers entirely to SO processes, i.e., ejection processes. In reality, this probability is divided in certain ratio between SU and SO processes. Despite this, the approximation used is justified for the following reasons. As direct calculations show [15, 16], the probabilities of Auger transitions with the participation of an electron that is additionally excited to Rydberg states are considerably smaller than probabilities of transitions without its participation. Then, as a result of subsequent transitions, this weakly bound electron can be ejected into the continuous spectrum with a high probability.

In formula (5), a correcting factor k is introduced. If overlap integrals are calculated using exact Hartree–Fock orbitals, this factor is unity. In this work, we use the following approximate analytical representation of overlap integrals [23]:

$$\langle nl[C_k] | nl[C_m] \rangle = \left[\frac{2\sqrt{r_k r_m}}{r_k + r_m} \right]^{2l+3}. \quad (6)$$

Here, r_k and r_m are the average Hartree–Fock radii of the nl orbital in configurations C_k and C_m. Investigation of the accuracy of approximation (6) that was performed upon calculations of probabilities of various shake processes in atoms of noble gases [15, 16] showed that it underestimates probability (5). It was found that exact values of $w(nl)$, which are obtained

Table 1. Electron configurations $\{C_i^{(0)}\}$ of the neon atomic core produced by the photoionization, photoionization channels that lead to these configurations, and energies E^{thr} of channel opening

Configuration		Photoionization channel	Energy, E^{thr}, eV
$C_1^{(0)}$	$1s^2 2s^2 2p^5$	$2p$-ionization	19.8
$C_2^{(0)}$	$1s^2 2s^1 2p^6$	$2s$-ionization	49.4
$C_3^{(0)}$	$1s^1 2s^2 2p^6$	single $1s$-ionization	869.6
$C_4^{(0)}$	$1s^1 2s^2 2p^5 3p^1$	$1s$-ionization with the $2p \to 3p$ SU-excitation	905.7
$C_5^{(0)}$	$1s^1 2s^2 2p^5 4p^1$	$1s$-ionization with the $2p \to 4p$ SU-excitation	910.9
$C_6^{(0)}$	$1s^1 2s^2 2p^5 5p^1$	$1s$-ionization with the $2p \to 5p$ SU-excitation	912.9
$C_7^{(0)}$	$1s^1 2s^2 2p^5$	$1s$-ionization with the SO-ejection $2p$-electron	915.8
$C_8^{(0)}$	$1s^1 2s^1 2p^6 3s^1$	$1s$-ionization with the $2s \to 3s$ SU-excitation	931.1
$C_9^{(0)}$	$1s^1 2s^1 2p^6 4s^1$	$1s$-ionization with the $2s \to 4s$ SU-excitation	938.7
$C_{10}^{(0)}$	$1s^1 2s^1 2p^6 5s^1$	$1s$-ionization with the $2s \to 5s$ SU-excitation	941.3
$C_{11}^{(0)}$	$1s^1 2s^1 2p^6$	$1s$-ionization with the SO-ejection of $2s$ electron	944.6

with Hartree–Fock wave functions, can be reproduced best at $k = 2$.

Let us return to the description of cascade decay. The probability of the $C_k - C_m$ transition is determined by a product of the probability of formation of initial configuration C_k of the transition, and the corresponding branching ratio,

$$P(C_k - C_m) = P(C_k)\chi(C_k - C_m). \quad (7)$$

The probability of formation of configuration C_k in the course of the development of the cascade is a product of probabilities of branching ratios of successive branches of the decay tree that go from initial configuration $C^{(0)}$ to a given decaying configuration C_k. If the C_k configuration can be reached via different pathways, its probability is defined as a sum of probabilities to reach C_k via all possible pathways,

$$P(C_k) = \sum_{\{a,b,..,p,q,k\}} \chi(C^{(0)} - C_a) \times \chi(C_a - C_b)\ldots\chi(C_p - C_q)\chi(C_q - C_k). \quad (8)$$

Energies of transitions are found as differences of total energies of the initial and final configurations calculated in the Hartree–Fock–Pauli approximation. In this case, we do not take into account the so-called postcollisional interaction of the photoelectron with Auger electrons that are formed at the first step of the decay and the interaction of electrons of the continuous spectrum that are emitted upon successive nonradiative transitions.

It was shown in [11, 23, 29] that the distribution of the probability of SO-electrons over the energy is strongly asymmetric—the probability noticeably differs from zero only at small energies of SO-electrons. Therefore, we assumed in this work that, in the case of radiative or nonradiative transitions accompanied by SO processes, the kinetic energy of an additionally ionized SO-electron is zero. Furthermore, in the electron spectrum, there is no low-energy range that corresponds to SO-electrons, while the satellite that corresponds to the transition to this state with an additional vacancy is represented by a single line.

As was mentioned above, photoionization of an inner shell of an atom can give rise to various excited states. Table 1 presents electron configurations $C_i^{(0)}$ of the neon atomic core that are formed as a result of photoionization, photoionization channels that lead to these configurations, and energies of channel opening (or thresholds) E^{thr}.

The probability of formation of any configuration $C_i^{(0)}$ as a result of photoionization depends on energy $\hbar\omega$ of the absorbed photon,

$$P(C_i^{(0)}, \hbar\omega) = \frac{\sigma_i(\hbar\omega)}{\sum_j \sigma_j(\hbar\omega)}, \quad (9)$$

where $\sigma_i(\hbar\omega)$ is the cross section of the ith channel of photoionization that leads to the formation of an excited state with configuration $C_i^{(0)}$, and summation is done over all photoionization channels that are possible at a given photon energy.

Table 2. Probabilities of most probable radiative transitions (including the transitions which are accompanied by the additional monopole SO-ejection of one outer electron) upon cascade decays of different configurations $C_i^{(0)}$ (see Table 1) produced by photoionization

Energy, eV	Initial configuration of transition	Final configuration of transition	Decaying configuration								
			$C_3^{(0)}$	$C_4^{(0)}$	$C_5^{(0)}$	$C_6^{(0)}$	$C_7^{(0)}$	$C_8^{(0)}$	$C_9^{(0)}$	$C_{10}^{(0)}$	$C_{11}^{(0)}$
0.50	$1s^22s^22p^45p^1$	$1s^22s^22p^45s^1$				0.0025					
0.64	$1s^22s^22p^45p^1$	$1s^22s^22p^44d^1$				0.0017					
0.77	$1s^22s^22p^35p^1$	$1s^22s^22p^35s^1$				0.0255					
1.13	$1s^22s^22p^44p^1$	$1s^22s^22p^44s^1$			0.0064	0.0002					
1.30	$1s^22s^22p^44d^1$	$1s^22s^22p^44p^1$				0.0002					
1.39	$1s^22s^22p^44p^1$	$1s^22s^22p^43d^1$			0.0025	0.0001					
1.43	$1s^22s^22p^45s^1$	$1s^22s^22p^44p^1$				0.0003					
1.66	$1s^22s^22p^34p^1$	$1s^22s^22p^34s^1$			0.0699	0.0014					
1.91	$1s^22s^22p^34d^1$	$1s^22s^22p^34p^1$				0.0033					
1.96	$1s^22s^22p^35p^1$	$1s^22s^22p^34d^1$				0.1391					
3.06	$1s^22s^22p^45p^1$	$1s^22s^22p^44s^1$				0.0009					
3.10	$1s^22s^22p^35s^1$	$1s^22s^22p^34p^1$				0.0051					
3.33	$1s^22s^22p^45p^1$	$1s^22s^22p^43d^1$				0.0027					
3.52	$1s^22s^22p^43p^1$	$1s^22s^22p^43s^1$		0.0152	0.0022	0.0016					
3.61	$1s^22s^22p^43d^1$	$1s^22s^22p^43p^1$			0.0006	0.0007					
3.87	$1s^22s^22p^44s^1$	$1s^22s^22p^43p^1$			0.0016	0.0003					
4.08	$1s^22s^22p^25p^1$	$1s^22s^22p^24d^1$				0.0005					
4.26	$1s^22s^22p^34p^1$	$1s^22s^22p^33d^1$			0.2430	0.0048					
4.79	$1s^22s^22p^33p^1$	$1s^22s^22p^33s^1$		0.4526	0.0453	0.0240					
5.29	$1s^22s^22p^33d^1$	$1s^22s^22p^33p^1$			0.0177	0.0083					
5.53	$1s^22s^22p^35p^1$	$1s^22s^22p^34s^1$				0.0151					
5.66	$1s^22s^22p^23p^1$	$1s^22s^22p^23s^1$		0.0016							
6.43	$1s^22s^22p^45s^1$	$1s^22s^22p^43p^1$				0.0006					
7.89	$1s^22s^22p^34s^1$	$1s^22s^22p^33p^1$			0.0276	0.0065					
8.12	$1s^22s^22p^35p^1$	$1s^22s^22p^33d^1$				0.1097					
8.52	$1s^22s^22p^44p^1$	$1s^22s^22p^43s^1$			0.0065	0.0002					
8.90	$1s^22s^22p^24p^1$	$1s^22s^22p^23d^1$			0.0006						
10.45	$1s^22s^22p^45p^1$	$1s^22s^22p^43s^1$				0.0075					
11.46	$1s^22s^22p^34d^1$	$1s^22s^22p^33p^1$				0.0018					
12.65	$1s^22s^22p^35s^1$	$1s^22s^22p^33p^1$				0.0073					
14.34	$1s^22s^22p^34p^1$	$1s^22s^22p^33s^1$			0.1066	0.0021					
15.18	$1s^22s^22p^25p^1$	$1s^22s^22p^23d^1$				0.0003					
18.21	$1s^22s^22p^35p^1$	$1s^22s^22p^33s^1$				0.1108					
22.54	$1s^22s^12p^3$	$1s^22s^22p^2$			0.0017	0.0017	0.0038	0.0023	0.0022	0.0017	0.0028
22.57	$1s^22s^12p^33p^1$	$1s^22s^22p^23p^1$		0.0007							
22.91	$1s^22s^12p^33s^1$	$1s^22s^22p^23s^1$						0.0003			
25.57	$1s^22s^12p^45p^1$	$1s^22s^22p^35p^1$				0.0002					

Table 2. (Contd.)

Energy, eV	Initial configuration of transition	Final configuration of transition	Decaying configuration								
			$C_3^{(0)}$	$C_4^{(0)}$	$C_5^{(0)}$	$C_6^{(0)}$	$C_7^{(0)}$	$C_8^{(0)}$	$C_9^{(0)}$	$C_{10}^{(0)}$	$C_{11}^{(0)}$
25.58	$1s^22s^12p^4$	$1s^22s^22p^3$	0.0034	0.1693	0.1925	0.2054	0.4577	0.3737	0.3269	0.3175	0.9783
26.91	$1s^22s^22p^25p^1$	$1s^22s^22p^23s^1$				0.0001					
27.77	$1s^22s^22p^43s^1$	$1s^22s^22p^5$		0.0152	0.0087	0.0093					
27.92	$1s^22s^12p^5$	$1s^22s^22p^4$	0.4073	0.0024	0.0009	0.0004		0.0049	0.0026	0.0013	0.0189
28.37	$1s^22p^4$	$1s^22s^12p^3$					0.0017	0.0011	0.0005	0.0003	0.0015
28.37	$1s^22p^43p^1$	$1s^22s^12p^33p^1$		0.0008							
28.76	$1s^22p^43s^1$	$1s^22s^12p^33s^1$						0.0004			
31.07	$1s^22p^55p^1$	$1s^22s^12p^45p^1$				0.0002					
31.07	$1s^22p^5$	$1s^22s^12p^4$	0.0013	0.0162	0.0255	0.0305	0.1290	0.0835	0.0513	0.0393	0.2018
33.10	$1s^22p^6$	$1s^22s^12p^5$	0.1043					0.0013	0.0008	0.0004	
34.89	$1s^22s^22p^43d^1$	$1s^22s^22p^5$			0.0019	0.0021					
35.15	$1s^22s^22p^44s^1$	$1s^22s^22p^5$			0.0048	0.0008					
37.58	$1s^22s^22p^44d^1$	$1s^22s^22p^5$				0.0015					
37.71	$1s^22s^22p^45s^1$	$1s^22s^22p^5$				0.0017					
41.44	$1s^22s^22p^33s^1$	$1s^22s^22p^4$		0.4526	0.1518	0.1369					
51.38	$1s^22p^43s^1$	$1s^22p^5$						0.0001			
51.53	$1s^22s^22p^33d^1$	$1s^22s^22p^4$			0.2253	0.1062					
53.69	$1s^22s^12p^33s^1$	$1s^22s^12p^4$		0.0001				0.0008			
54.12	$1s^22s^22p^34s^1$	$1s^22s^22p^4$			0.0424	0.0100					
56.36	$1s^22s^22p^23s^1$	$1s^22s^22p^3$		0.0016	0.0001	0.0002		0.0003			
57.69	$1s^22s^22p^34d^1$	$1s^22s^22p^4$				0.1340					
58.88	$1s^22s^22p^35s^1$	$1s^22s^22p^4$				0.0131					
68.10	$1s^22s^22p^23d^1$	$1s^22s^22p^3$			0.0006	0.0003					
79.20	$1s^22s^22p^24d^1$	$1s^22s^22p^3$				0.0005					
84.60	$1s^22s^12p^33p^1$	$1s^22s^22p^3$		0.0023							
87.40	$1s^22p^43p^1$	$1s^22s^12p^4$		0.0011							
780.78	$1s^12s^22p^6$	$1s^22s^12p^5$	0.0001								
789.33	$1s^12s^22p^5$	$1s^22s^22p^3$					0.0012	0.0007	0.0004	0.0002	
792.39	$1s^12s^22p^55p^1$	$1s^22s^22p^35p^1$				0.0012					
792.59	$1s^12s^12p^6$	$1s^22s^12p^4$									0.0017
794.25	$1s^12s^22p^54p^1$	$1s^22s^22p^34p^1$			0.0012						
795.91	$1s^12s^12p^65s^1$	$1s^22s^12p^45s^1$								0.0014	
798.04	$1s^12s^12p^64s^1$	$1s^22s^12p^44s^1$							0.0012		
798.56	$1s^12s^22p^53p^1$	$1s^22s^22p^33p^1$		0.0012							
803.01	$1s^12s^12p^63s^1$	$1s^22s^12p^43s^1$						0.0007			
808.69	$1s^12s^22p^6$	$1s^22s^22p^4$	0.0022								
844.80	$1s^12s^22p^53p^1$	$1s^22s^22p^4$		0.0001							
849.73	$1s^12s^22p^6$	$1s^22s^22p^5$	0.0174								

Table 2. (Contd.)

Energy, eV	Initial configuration of transition	Final configuration of transition	Decaying configuration								
			$C_3^{(0)}$	$C_4^{(0)}$	$C_5^{(0)}$	$C_6^{(0)}$	$C_7^{(0)}$	$C_8^{(0)}$	$C_9^{(0)}$	$C_{10}^{(0)}$	$C_{11}^{(0)}$
854.55	$1s^12s^22p^53p^1$	$1s^22s^22p^43p^1$		0.0152							
854.79	$1s^12s^22p^54p^1$	$1s^22s^22p^44p^1$			0.0154						
854.86	$1s^12s^22p^55p^1$	$1s^22s^22p^45p^1$				0.0154					
854.92	$1s^12s^22p^5$	$1s^22s^22p^4$					0.0154	0.0096	0.0047	0.0024	
855.50	$1s^12s^12p^63s^1$	$1s^22s^12p^53s^1$						0.0070			
855.73	$1s^12s^12p^64s^1$	$1s^22s^12p^54s^1$							0.0130		
855.79	$1s^12s^12p^65s^1$	$1s^22s^12p^55s^1$								0.0160	
855.83	$1s^12s^12p^6$	$1s^22s^12p^5$									0.0189

Let $Spect(C_i^{(0)})$ be the spectrum produced by the cascade decay of one initial configuration $C_i^{(0)}$. Since different configurations $\{C_i^{(0)}\}$ can be formed upon photoionization, the spectrum at a given energy of incident photons is a superposition

$$Spect(\hbar\omega) = \sum_i P(C_i^{(0)}, \hbar\omega) Spect(C_i^{(0)}). \qquad (10)$$

The 1*s*-, 2*s*-, and 2*p*-photoionization cross sections of the neon atom were calculated taking into account the rearrangement effect (relaxation) of the atomic core in the potential of a vacancy that is formed upon photoionization [30].

The cross section of the 1*s*-photoionization, which is accompanied by the $2l \to nl$ SU-excitation, was found as a product of 1*s*-photoionization cross section σ_{1s} and the relative probability of the corresponding SU process,

$$\sigma^{SU}_{1s,2l\to nl}(\hbar\omega) = w_{SU}(1s, 2l \to nl)\sigma_{1s}(\hbar\omega - (E^{thr}_{1s,2l\to nl} - E^{thr}_{1s})), \qquad (11)$$

where E_{1s}^{thr} is the threshold of the 1*s*-ionization, $E_{1s,2l\to nl}^{thr}$ is the threshold energy of the 1*s*-photoionization accompanied by the $2l \to nl$ SU excitation. In accordance with [11], the relative probabilities of the $2l \to nl$ SU-excitations caused by the creation of the 1*s*-vacancy in the neon atom were calculated by the formula

$$w_{SU}(1s, 2l \to nl) = \frac{N_{2l}\left\langle nl[1s^{-1}]\middle|2l[0]\right\rangle^2}{\left\langle 2l[1s^{-1}]\middle|2l[0]\right\rangle^2}. \qquad (12)$$

Here, configurations in which the corresponding orbitals were optimized are indicated in square brackets as follows: $[0] \equiv 1s^22s^22p^6$, $[1s^{-1}] \equiv 1s^12s^22p^6$; N_{2l} is the number of electrons in the $2l$ subshell in configuration [0] ($N_{2s} = 2$, $N_{2p} = 6$).

In the case of the 1*s*-photoionization accompanied by the $2l$ SO-ejection, it is necessary to take into account all possible energies of the SO-electron. Therefore, the cross section of this process is the integral

$$\sigma^{SO}_{1s,2l}(\hbar\omega) = \int_0^{\hbar\omega - E^{thr}_{1s,2l}} w_{SO}(1s, 2l \to \varepsilon l) \times \sigma_{1s}(\hbar\omega - (E^{thr}_{1s,2l} - E^{thr}_{1s}) - \varepsilon)d\varepsilon, \qquad (13)$$

where $w_{SO}(1s, 2l \to \varepsilon l)$ is the probability density of $2l \to \varepsilon l$ SO-processes caused by the creation of the 1*s*-vacancy,

$$w_{SO}(1s, 2l \to \varepsilon l) = \frac{N_{2l}\left\langle \varepsilon l[1s^{-1}]\middle|2l[0]\right\rangle^2}{\left\langle 2l[1s^{-1}]\middle|2l[0]\right\rangle^2}. \qquad (14)$$

Note that, in contrast to the calculation of probabilities of shake processes that accompany intraatomic diagram transitions (formulas (5), (6)), integrals in (12) and (14) were calculated using exact Hartree–Fock orbitals.

In this work, we did not consider some high-order processes, which can give rise to additional configurations $C_i^{(0)}$ (compared to those presented in Table 1) and/or modify decay trees, namely:

• multiple monopole shake processes, which result in additional excitation and/or ionization of more than one outer electron;

• nonmonopole shake processes (conjugate shake processes), in which one of inner electrons is knocked out by an outgoing photoelectron;

• double Auger processes, in which an atom emits two electrons as a result of one nonradiative transition.

Table 3. Probabilities of most probable nonradiative transitions (Auger and Coster–Kronig processes, including processes which are accompanied by the additional monopole SO-ejection of one outer electron) upon cascade decays of different configurations $C_i^{(0)}$ (see Table 1) produced by photoionization

Energy, eV	Initial configuration of transition	Final configuration of transition	Decaying configuration								
			$C_3^{(0)}$	$C_4^{(0)}$	$C_5^{(0)}$	$C_6^{(0)}$	$C_7^{(0)}$	$C_8^{(0)}$	$C_9^{(0)}$	$C_{10}^{(0)}$	$C_{11}^{(0)}$
1.67	$1s^22s^12p^43s^1$	$1s^22s^22p^3$						0.2765			
4.28	$1s^22s^12p^34s^1$	$1s^22s^22p^2$							0.0011		
6.21	$1s^22s^12p^43p^1$	$1s^22s^22p^3$		0.2843							
6.26	$1s^22s^12p^34p^1$	$1s^22s^22p^2$			0.0021						
7.42	$1s^22p^53s^1$	$1s^22s^12p^4$						0.0721			
10.23	$1s^22p^44s^1$	$1s^22s^12p^3$							0.0010		
11.59	$1s^22s^12p^35s^1$	$1s^22s^22p^2$								0.0011	
11.66	$1s^22p^53p^1$	$1s^22s^12p^4$		0.1111							
12.09	$1s^22p^44p^1$	$1s^22s^12p^3$			0.0017						
12.53	$1s^22s^12p^35p^1$	$1s^22s^22p^2$				0.0023					
14.18	$1s^22s^12p^44s^1$	$1s^22s^22p^3$							0.4893		
14.77	$1s^22s^12p^53s^1$	$1s^22s^22p^4$						0.0070			
15.35	$1s^12s^12p^63s^1$	$1s^12s^22p^5$						0.6224			
15.77	$1s^22s^12p^44p^1$	$1s^22s^22p^3$			0.2634						
17.47	$1s^22p^45s^1$	$1s^22s^12p^3$								0.0011	
18.36	$1s^22p^45p^1$	$1s^22s^12p^3$				0.0017					
18.90	$1s^22s^12p^45s^1$	$1s^22s^22p^3$								0.5796	
19.64	$1s^22s^12p^45p^1$	$1s^22s^22p^3$				0.2511					
19.75	$1s^22p^54s^1$	$1s^22s^12p^4$							0.1276		
21.26	$1s^22p^54p^1$	$1s^22s^12p^4$			0.1029						
22.07	$1s^22s^12p^54s^1$	$1s^22s^22p^4$							0.0130		
22.89	$1s^12s^12p^64s^1$	$1s^12s^22p^5$							0.3060		
24.43	$1s^22p^55s^1$	$1s^22s^12p^4$								0.1512	
24.61	$1s^22s^12p^55s^1$	$1s^22s^22p^4$								0.0160	
25.13	$1s^22p^55p^1$	$1s^22s^12p^4$				0.0980					
25.48	$1s^12s^12p^65s^1$	$1s^12s^22p^5$								0.1534	
645.11	$1s^12s^22p^5$	$1s^22p^4$					0.0017	0.0011	0.0005	0.0003	
652.25	$1s^12s^22p^55p^1$	$1s^22p^45p^1$				0.0017					
656.52	$1s^12s^22p^54p^1$	$1s^22p^44p^1$			0.0017						
666.24	$1s^12s^22p^53p^1$	$1s^22p^43p^1$		0.0018							
673.48	$1s^12s^22p^5$	$1s^22s^12p^3$					0.0020	0.0013	0.0006	0.0003	
673.95	$1s^12s^12p^6$	$1s^22p^4$									0.0015
680.62	$1s^12s^22p^55p^1$	$1s^22s^12p^35p^1$				0.0023					
681.50	$1s^12s^12p^65s^1$	$1s^22p^45s^1$								0.0011	
684.89	$1s^12s^22p^54p^1$	$1s^22s^12p^34p^1$			0.0021						
686.14	$1s^12s^12p^64s^1$	$1s^22p^44s^1$							0.0010		
686.46	$1s^12s^22p^6$	$1s^22p^5$	0.0013								

Table 3. (Contd.)

Energy, eV	Initial configuration of transition	Final configuration of transition	Decaying configuration								
			$C_3^{(0)}$	$C_4^{(0)}$	$C_5^{(0)}$	$C_6^{(0)}$	$C_7^{(0)}$	$C_8^{(0)}$	$C_9^{(0)}$	$C_{10}^{(0)}$	$C_{11}^{(0)}$
694.61	$1s^12s^22p^53p^1$	$1s^22s^12p^33p^1$		0.0023							
696.03	$1s^12s^22p^5$	$1s^22s^22p^2$					0.0008	0.0005	0.0002	0.0001	0
696.65	$1s^12s^12p^63s^1$	$1s^22p^43s^1$						0.0006			
702.32	$1s^12s^12p^6$	$1s^22s^12p^3$									0.0013
703.18	$1s^12s^22p^55p^1$	$1s^22s^22p^25p^1$				0.0009					
707.45	$1s^12s^22p^54p^1$	$1s^22s^22p^24p^1$			0.0007						
709.93	$1s^12s^12p^65s^1$	$1s^22s^12p^35s^1$								0.0011	
714.63	$1s^12s^12p^64s^1$	$1s^22s^12p^34s^1$							0.0011		
717.19	$1s^12s^22p^53p^1$	$1s^22s^22p^23p^1$		0.0009							
717.53	$1s^12s^22p^6$	$1s^22s^12p^4$	0.0021								
722.56	$1s^12s^22p^53p^1$	$1s^22p^5$		0.0162							
725.41	$1s^12s^12p^63s^1$	$1s^22s^12p^33s^1$						0.0006			
727.81	$1s^12s^22p^54p^1$	$1s^22p^5$			0.0255						
729.81	$1s^12s^22p^55p^1$	$1s^22p^5$				0.0305					
732.69	$1s^12s^22p^5$	$1s^22p^5$					0.1290	0.0803	0.0395	0.0198	
735.75	$1s^12s^22p^55p^1$	$1s^22p^55p^1$				0.0982					
737.62	$1s^12s^22p^54p^1$	$1s^22p^54p^1$			0.1030						
741.97	$1s^12s^22p^53p^1$	$1s^22p^53p^1$		0.1111							
743.11	$1s^12s^22p^6$	$1s^22s^22p^3$	0.0008								
747.67	$1s^12s^22p^6$	$1s^22p^6$	0.1043								
748.03	$1s^12s^12p^63s^1$	$1s^22p^5$						0.0031			
753.64	$1s^12s^22p^53p^1$	$1s^22s^12p^4$		0.0408							
755.57	$1s^12s^12p^64s^1$	$1s^22p^5$							0.0119		
758.17	$1s^12s^12p^65s^1$	$1s^22p^5$								0.0195	
758.88	$1s^12s^22p^54p^1$	$1s^22s^12p^4$			0.0641						
760.88	$1s^12s^22p^55p^1$	$1s^22s^12p^4$				0.0769					
761.52	$1s^12s^12p^6$	$1s^22p^5$									0.2017
763.76	$1s^12s^22p^5$	$1s^22s^12p^4$					0.3286	0.2046	0.1006	0.0504	
764.81	$1s^12s^12p^65s^1$	$1s^22p^55s^1$								0.1512	
766.81	$1s^12s^22p^55p^1$	$1s^22s^12p^45p^1$				0.2510					
766.89	$1s^12s^12p^64s^1$	$1s^22p^54s^1$							0.1276		
768.68	$1s^12s^22p^54p^1$	$1s^22s^12p^44p^1$			0.2633						
771.69	$1s^12s^12p^63s^1$	$1s^22p^53s^1$						0.0721			
773.01	$1s^12s^22p^53p^1$	$1s^22s^12p^43p^1$		0.2842							
779.10	$1s^12s^12p^63s^1$	$1s^22s^12p^4$						0.0127			
779.21	$1s^12s^22p^53p^1$	$1s^22s^22p^3$		0.0642							
780.78	$1s^12s^22p^6$	$1s^22s^12p^5$	0.3029								
784.45	$1s^12s^22p^54p^1$	$1s^22s^22p^3$			0.1011						
786.45	$1s^12s^22p^55p^1$	$1s^22s^22p^3$				0.1213					

Table 3. (Contd.)

Energy, eV	Initial configuration of transition	Final configuration of transition	Decaying configuration								
			$C_3^{(0)}$	$C_4^{(0)}$	$C_5^{(0)}$	$C_6^{(0)}$	$C_7^{(0)}$	$C_8^{(0)}$	$C_9^{(0)}$	$C_{10}^{(0)}$	$C_{11}^{(0)}$
786.64	$1s^12s^12p^64s^1$	$1s^22s^12p^4$							0.0473		
789.24	$1s^12s^12p^65s^1$	$1s^22s^12p^4$								0.0766	
789.33	$1s^12s^22p^5$	$1s^22s^22p^3$					0.5212	0.3244	0.1595	0.0800	
792.39	$1s^12s^22p^55p^1$	$1s^22s^22p^35p^1$				0.3988					
792.59	$1s^12s^12p^6$	$1s^22s^12p^4$									0.7748
794.25	$1s^12s^22p^54p^1$	$1s^22s^22p^34p^1$			0.4182						
795.91	$1s^12s^12p^65s^1$	$1s^22s^12p^45s^1$								0.5782	
798.04	$1s^12s^12p^64s^1$	$1s^22s^12p^44s^1$							0.4880		
798.56	$1s^12s^22p^53p^1$	$1s^22s^22p^33p^1$		0.4514							
803.01	$1s^12s^12p^63s^1$	$1s^22s^12p^43s^1$						0.2758			
808.69	$1s^12s^22p^6$	$1s^22s^22p^4$	0.5688								
809.25	$1s^12s^12p^63s^1$	$1s^22p^6$						0.0013			
816.78	$1s^12s^12p^64s^1$	$1s^22p^6$							0.0008		
816.88	$1s^12s^22p^53p^1$	$1s^22s^12p^5$		0.0024							
819.38	$1s^12s^12p^65s^1$	$1s^22p^6$								0.0004	
822.12	$1s^12s^22p^54p^1$	$1s^22s^12p^5$			0.0009						
824.12	$1s^12s^22p^55p^1$	$1s^22s^12p^5$				0.0004					
842.35	$1s^12s^12p^63s^1$	$1s^22s^12p^5$						0.0036			
844.80	$1s^12s^22p^53p^1$	$1s^22s^22p^4$		0.0077							
849.89	$1s^12s^12p^64s^1$	$1s^22s^12p^5$							0.0019		
850.04	$1s^12s^22p^54p^1$	$1s^22s^22p^4$			0.0026						
852.04	$1s^12s^22p^55p^1$	$1s^22s^22p^4$				0.0013					
852.48	$1s^12s^12p^65s^1$	$1s^22s^12p^5$								0.0009	

A detailed discussion of probabilities of these processes in the neon atom can be found in [21]. Here, we only note that some of these processes are of comparable significance to less probable processes that were taken into account in this work. In particular, this concerns double *K*–*LLL* Auger processes, the probability of which is about 5–6% of the total probability of the *K* Auger emission [31, 32]. However, consistent and accurate consideration of the influence of these processes on cascade decay is a very complicated problem and deserves a separate investigation.

RESULTS AND DISCUSSION

For each excited state of the neon atom with core configuration $C_i^{(0)}$ (see Table 1) that is formed upon photoionization, the decay trees are built, as was described in the preceding section. When building a decay tree, we neglected the branches that correspond to transitions with probability (7) smaller than 10^{-7}. Investigations of the influence of the detailedness of description of the cascade on the calculation accuracy showed [23] that this threshold value is quite justified: further decrease in the threshold value does not practically affect the results of calculation of cascade characteristics.

Tables 2 and 3 present probabilities of radiative and nonradiative transitions upon cascade decays of particular excited states created by photoionization, which were calculated by the formulas (7) and (8). It should be noted that the configurations of the initial and final states of transitions listed in Tables 2 and 3 do not always correspond to diagram transitions. This is related to the fact that the tables also contain transitions that are accompanied by the SO-ejection of one of the outer electrons. In Tables 2 and 3, we present only the most probable transitions, the probabilities of

which (upon decay of at least one of configurations $C_i^{(0)}$) exceed 10^{-4}.

Table 4 contains probabilities of formation of Ne^{q+} ions of different charges created as a result of the decay of configurations $C_i^{(0)}$.

Since the state with configuration $C_1^{(0)} \equiv 1s^22s^22p^5$ is not subjected to decay and the state with $C_2^{(0)} \equiv 1s^22s^12p^6$ decays through only the radiative $2s$–$2p$ transition ($L_1L_{2,3}L_{2,3}$ super-Coster–Kronig processes in neon are energetically forbidden [16], while the probability of additional SO upon the $2s$–$2p$ transition is small), the spectra created by the decay of these states are not presented in Tables 2–4.

Let us briefly discuss the probabilities of formation of Ne^{q+} ions upon decays of different $C_i^{(0)}$ (Table 4). The decay of the state with configuration $C_3^{(0)} \equiv 1s^12s^22p^6$ leads to the formation of the Ne^{2+} ion with a very high probability (97.8%), because main channels of the decay of this state are *KLL* Auger transitions. A singly charged Ne^{1+} ion is formed as a result of the $1s$–$2p$ radiative transition (1.8%). The formation of triply charged Ne^{3+} ions (0.4%) is caused by additional SO-ejections of either $2s$ or $2p$ electron upon *KLL* Auger transitions.

As was expected, the occurrence of an additional vacancy in the L shell in configurations $C_7^{(0)} \equiv 1s^12s^22p^5$ and $C_{11}^{(0)} \equiv 1s^12s^12p^6$ leads, figuratively speaking, to a mere shift of the charge spectrum by +1, with the relative probabilities of ion formation remaining almost unchanged.

Let us consider the decay of configurations $\{C_k^{(0)}\}_{k=8,9,10} \equiv 1s^12s^12p^6\{ns^1\}_{n=3,4,5}$. At the first step, main decay channels of these configurations are *KLL* Auger transitions and $L_1L_{2,3}\{M_1, N_1, O_1\}$ Coster–Kronig transitions, respectively. Furthermore, as n increases, Auger processes play a greater role. Thus, whereas upon the decay of configuration $C_8^{(0)} \equiv 1s^12s^12p^63s^1$, the $L_1L_{2,3}M_1$ Coster–Kronig transition predominates at the first step ($L_1L_{2,3}M_1$ branching probability is 62.2%, while that of *KLL* is 34.8%), upon the decay of configuration $C_{10}^{(0)} \equiv 1s^12s^12p^65s^1$, *KLL* Auger transitions are most probable ($L_1L_{2,3}M_1$—15.3% versus *KLL*—72.9%). At the second step of the decay, configurations that arose as a result of *KLL* Auger transitions decay via Coster–Kronig transitions with an overwhelming probability, while the configuration that was formed as a result of the Coster–Kronig transition decays via *KLL* Auger transitions. Configurations that were formed as a result of two successive nonradiative transitions, are either not subjected to further decay or decay radiatively. Therefore, the most probable final charge state of the neon ion is Ne^{3+}. *KLL*/SO*ns* Auger transitions that occur at the first step of the decay and that are accompanied by the SO-ejection of a weakly bound *ns* electron also contribute to the probability of Ne^{3+} ion formation. In this case, the probability of these processes increases with n, so that, in the end, the decay of configurations $1s^12s^12p^6\{ns^1\}_{n=3,4,5}$ yields Ne^{3+} with a probability of ≈97.6% (Table 4).

Table 4. Probabilities of formation of Ne^{q+} ions as a result of cascade decays of different configurations $C_i^{(0)}$ (see Table 1) which are formed upon photoionization

Decaying configuration		Ion charge			
		1+	2+	3+	4+
$C_3^{(0)}$	$1s^12s^22p^6$	0.018	0.978	0.004	0.000
$C_4^{(0)}$	$1s^12s^22p^53p^1$	0.015	0.463	0.522	0.000
$C_5^{(0)}$	$1s^12s^22p^54p^1$	0.015	0.423	0.558	0.004
$C_6^{(0)}$	$1s^12s^22p^55p^1$	0.015	0.402	0.579	0.004
$C_7^{(0)}$	$1s^12s^22p^5$	0.000	0.015	0.980	0.005
$C_8^{(0)}$	$1s^12s^12p^63s^1$	0.000	0.021	0.976	0.003
$C_9^{(0)}$	$1s^12s^12p^64s^1$	0.000	0.020	0.976	0.004
$C_{10}^{(0)}$	$1s^12s^12p^65s^1$	0.000	0.020	0.977	0.003
$C_{11}^{(0)}$	$1s^12s^12p^6$	0.000	0.019	0.978	0.003

Upon the decay of configurations $\{C_k^{(0)}\}_{k=4,5,6} \equiv 1s^12s^22p^5\{np^1\}_{n=3,4,5}$, at the first step, *KLL* and *KLL*/SO*np* Auger transitions are the main decay channels. The KL_1L_1 and $KL_1L_{2,3}$ transitions lead to the formation of configurations with a vacancy in the $2s$ subshell, which decays with overwhelming probability via $L_1L_{2,3}\{M_{2,3}, N_{2,3}, O_{2,3}\}$ Coster–Kronig transitions at the second step. The $KL_{2,3}L_{2,3}$ transition gives the configurations which decay further only radiatively. Therefore, the probabilities of Ne^{2+} and Ne^{3+} ion formation due to decay of considered configurations are mainly determined by branching ratios of different *KLL* Auger transitions at the first step of the cascade and are comparable in magnitude (Table 4). Note that, the Auger transitions accompanied by the SO-ejection contribute to the formation of Ne^{3+} ions.

Figure 1 shows the cross sections of different photoionization channels of the neon atom that were calculated by formulas (11)–(14) in the near-K-threshold range (Rydberg structures corresponding to $1s \to np$ photoexcitations with $n \geqslant 3$ are not shown). Let us briefly discuss photoionization processes of the $1s$ subshell, accompanied by different SU/SO processes. We will denote these processes as $1s/\mathrm{SU}2l \to n'l$ in the case of the SU excitation of a $2l$ electron to an $n'l$ state

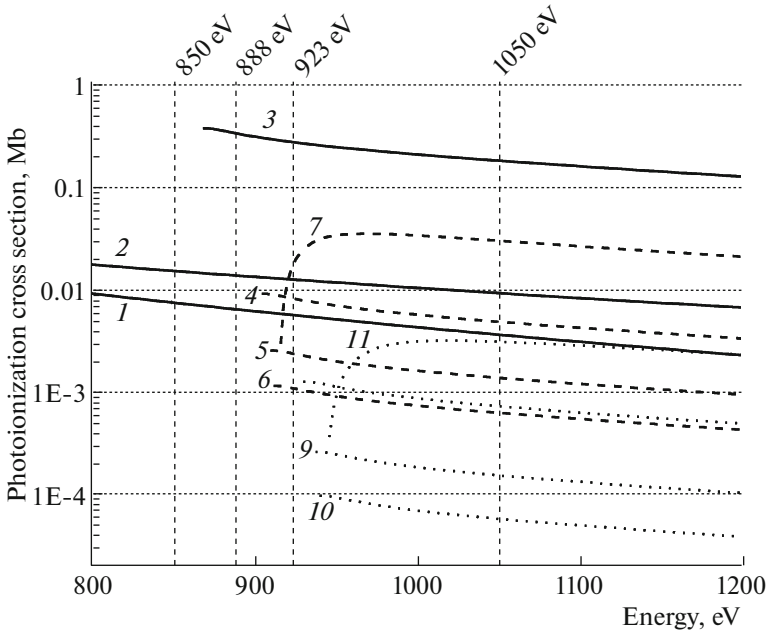

Fig. 1. Cross sections of different photoionization channels of the neon atom: (*1*) 2*p*-ionization, (*2*) 2*s*-ionization, (*3*) 1*s*-ionization, (*4*) 1*s*/SU2*p* → 3*p*, (*5*) 1*s*/SU2*p* → 4*p*, (*6*) 1*s*/SU2*p* → 5*p*, (*7*) 1*s*/SO2*p*, (*8*) 1*s*/SU2*s* → 3*s*, (*9*) 1*s*/SU2*s* → 4*s*, (*10*) 1*s*/SU2*s* → 5*s*, and (*11*) 1*s*/SO2*s* (the shake process which accompanies photoionization is indicated behind the slash). Vertical dashed lines indicate the photon energies for which, in this work, the cascade-produced spectra were calculated.

and as 1*s*/SO2*l* in the case of the SO-ejection of a 2*l* electron ($n' = 3, 4, 5$; $l = s, p$). As follows from (11), cross sections of 1*s*/SU2*l* → *n*'*l* processes are similar in shape to the cross section of the single 1*s*-photoionization, differing only in intensity and threshold energy. The energy dependence of the cross sections of 1*s*/SO2*l* processes is different; namely, near the threshold, the cross section is small, then it gradually increases with energy, achieves a maximal value, and, after that, decreases. It is clear that the relative roles played by SU and SO processes depend on the energy of the absorbed photon. It is seen from Fig. 1 that, near the threshold of the 1*s*/SO2*l* channel, 1*s*/SU2*l* → *n*'*l* processes predominate; however, with the increase of energy, their relative role decreases and, far from the threshold, the 1*s*/SO2*l* process becomes already more probable. Along with this, the relative role played by 1*s*/SU2*l* → *n*'*l* processes decreases with increasing *n*'.

Processes of 1*s*-photoionization that are accompanied by excitation/ejection of the 2*p* electron are more probable compared to similar processes with the 2*s* electron. Moreover, 1*s*/SU2*p* → 4*p* and 1*s*/SU2*p* → 5*p* processes prove to be of the same order with the 1*s*/SU2*s* → 3*s* process. This undoubtedly is one of the basic arguments in favor of extending the list of photoionization channels under consideration compared to our previous calculation [21].

In order to show how different SU/SO processes that accompany the photoionization of the 1*s* shell of the neon atom affect the cascade-produced spectra of photons and Auger electrons and the charge spectra of ion yields, these spectra were calculated for the following energies of incident photons (in the parentheses, after each energy value, new photoionization channels which are opened at this energy are indicated):

- 850 eV (only 2*p*- and 2*s*-ionization processes are possible);
- 888 eV (single 1*s*-ionization can occur);
- 923 eV (1*s*/SU2*p* → *n*'*p* and 1*s*/SO2*p* processes can take place);
- 1050 eV (1*s*/SU2*s* → *n*'*s* and 1*s*/SO2*s* processes can proceed).

We note that these energies do not fall into the ranges of 1*s* → *np* excitations.

Figures 2–4 present the calculated spectra of photons and Auger electrons and the charge spectra of ion yields produced by the cascade decay of excited states which are formed as a result of photoionization of the neon atom at incident photon energies presented above. For comparison, these figures also show the results from [21], where 1*s*-photoionization channels of the 1*s*/SU2*l* → *n*'*l* type were considered only for $n' = 3$, and the decay trees were calculated without taking into account the SO processes accompanying the diagram transitions.

Consider photon emission spectra (Fig. 2). Figure 2a presents results of our previous calculation [21] and Fig. 2b shows results of this work. We will discuss the latter results, turning to previous ones only if

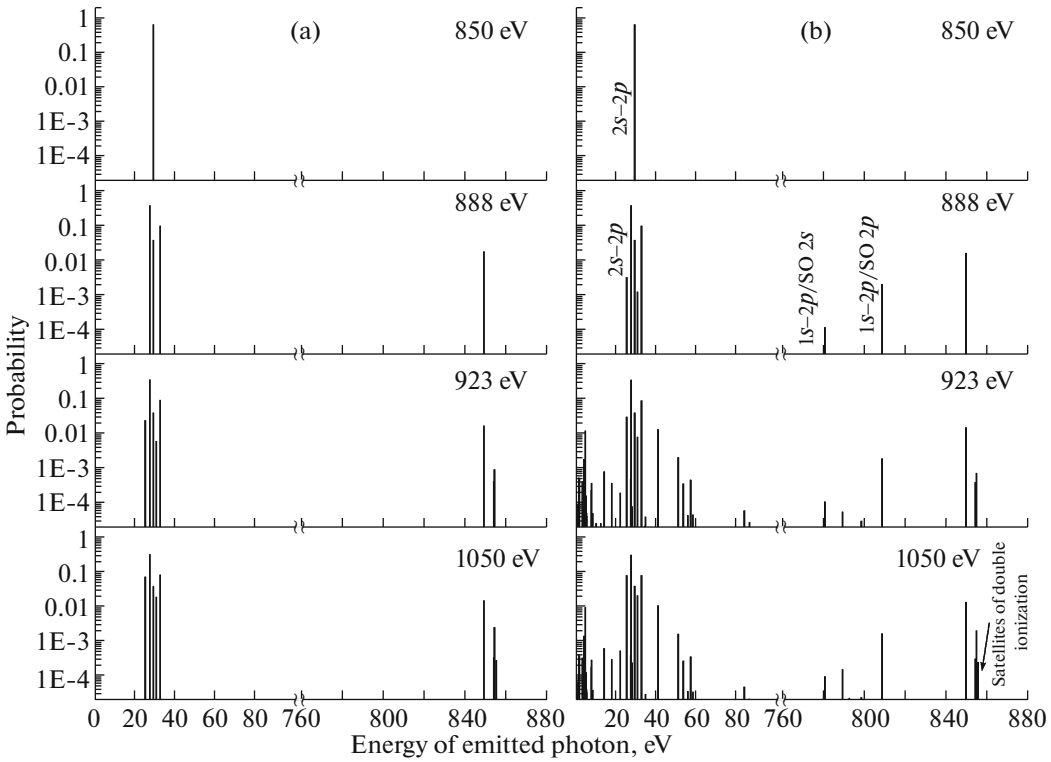

Fig. 2. Spectra of photons emitted upon cascade decays of excited states of the neon atom which are formed as a result of photoionization at different energies of incident photons: (a) results of calculations from [21] and (b) results of this work. Incident photon energy at which each spectrum was calculated is shown in the top right-hand corner.

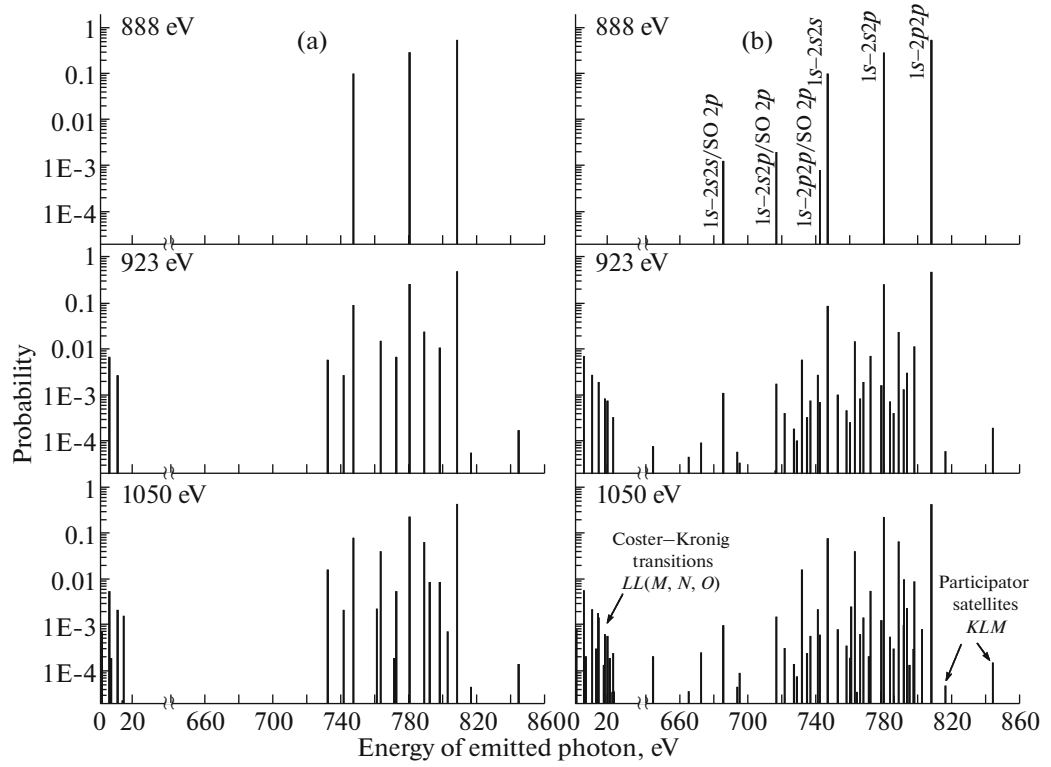

Fig. 3. Spectra of Auger electrons emitted upon cascade decays of excited states of the neon atom which are formed as a result of photoionization at different energies of incident photons: (a) results of calculations from [21] and (b) results of this work. Incident photon energy at which each spectrum was calculated is shown in the top left-hand corner.

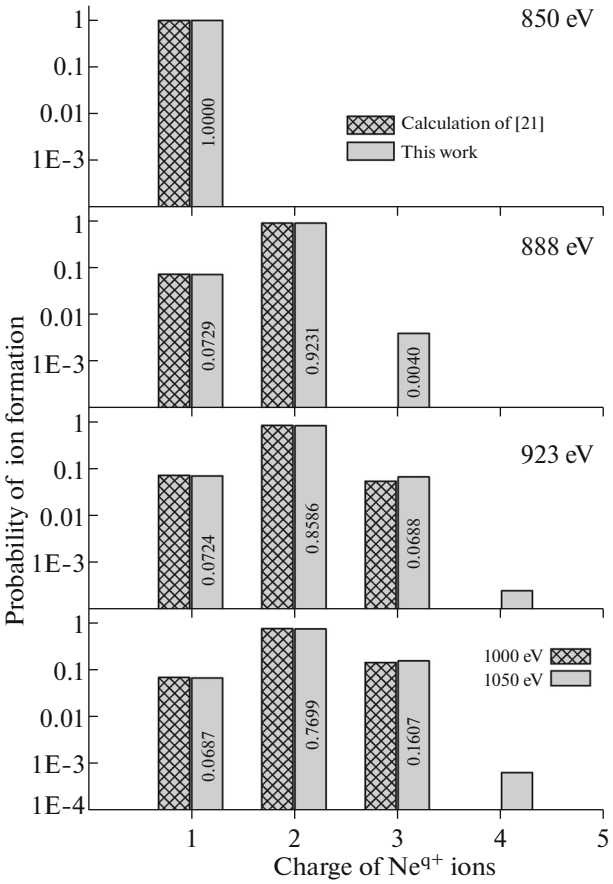

Fig. 4. Charge spectra of yields of Ne^{q+} ions that are formed upon cascade decays of excited states arising as a result of photoionization at different energies of incident photons. Hatched bars represent results of calculations from [21]; unhatched bars show results of calculations of this work. Incident photon energy at which each spectrum was calculated is shown in the top right-hand corner. Figures in bars that show calculation results of this work indicate probabilities of formation of ions with corresponding charges. The probability scale is logarithmic.

necessary to indicate their differences. At an energy of incident photons of 850 eV (only 2*p*- and 2*s*-photoionization processes are possible), the emission spectrum contains only one line (at 29.6 eV), and it corresponds to a photon which is emitted upon radiative transition of an electron from the 2*p* subshell to a vacancy in the 2*s* subshell which is formed as a result of the 2*s*-photoionization. At an energy of incident photons of 888 eV (single 1*s*-photoionization is also possible), the emission spectrum exhibits (i) a diagram line at 849.7 eV, which corresponds to the 1*s*–2*p* transition; (ii) two satellite components of this line (at 780.8 and 808.7 eV), which correspond to the 1*s*–2*p* transitions accompanied by additional 1*s*–2*p*/SO2*l* ($l = s$ and p) SO-ejections; and (iii) an increase in the number of 2*s*–2*p* lines, which is caused by transitions between different hole-configurations arising in the course of the cascade decay development of the 1*s* vacancy.

Let us dwell on changes of the emission spectrum that are caused by opening of shake channels of the 1*s*-photoionization. As can be seen (in Fig. 2b at energies of incident photons of 923 and 1050 eV), the opening of shake channels of the 1*s*-photoionization leads to the appearance of high-energy satellite components of the 1*s*–2*p* line (at ≈855 eV), which are caused by 1*s*–2*p* transitions in configurations with electrons of the 2*s* and 2*p* subshells additionally ionized/excited upon photoionization. In the literature, satellites of this type are referred to as satellites of double ionization. However, it should be noted that these satellites can be caused not only by double ionization, but also by ionization with an additional SU excitation.

In addition, the opening of photoionization shake channels leads to the increase in the number of 2*s*–2*p* lines and to the appearance of new lines in the low-energy range of the spectrum. These lines are caused by radiative transitions where an electron additionally SU-excited upon photoionization undergoes from high-energy Rydberg states at final stages of the cascade development. As can be seen (Fig. 2a), they were absent in the calculations of [21].

Let us now consider Auger electron spectra (Fig. 3b). At an energy of incident photons of 888 eV (single 1*s*-photoionization is possible, but shake channels are closed), the spectrum contains three diagram lines, which correspond to the KL_1L_1 (747.7 eV), $KL_1L_{2,3}$ (780.8 eV), and $KL_{2,3}L_{2,3}$ (808.7 eV) Auger transitions, and three of their low-energy satellite lines, which are caused by an additional SO-ejection of the 2*p* electron upon given transitions (clearly, they were not present in [21]; Fig. 3a).

The opening of 1*s*-photoionization shake channels leads to a substantial complication of the Auger electron spectrum (Fig. 3b at energies of incident photons of 923 and 1050 eV).

The decay of configurations which contain an electron additionally SU-excited upon photoionization produces satellites of two types in the Auger electron spectrum. Satellites of the first type are so-called spectator satellites and are caused by transitions in which the electron additionally SU-excited to a Rydberg state does not change its state in the Auger transition. These satellites lie in low-energy ranges with respect to diagram *KLL* lines and are rather close to satellites of double ionization. Satellites of the second type are so-called participator satellites, which are caused by the transitions in which an additionally SU-excited electron participates in the Auger transition. These satellites are located in high-energy ranges with respect to diagram *KLL* lines.

On the ground of considerations of the spatial localization of orbitals and the structure of integrals, which determine the amplitudes of Auger transitions,

it is clear that the probabilities of participator satellites should be considerably smaller than those of spectator satellites [23], which is observed in calculated spectra (Fig. 3b). In this case, with an increase in the average radius of a shell in which a Rydberg electron is located, the probability of a corresponding participator transition decreases rather rapidly. Therefore, among the $KL\{M, N, O\}$ Auger transitions that are possible in our case, we observe only KLM transitions in the Auger electron spectrum (Fig. 3b; two lines at 816.9 and 844.8 eV).

We also note another important particular feature of Auger electron spectra (Fig. 3b), which manifests itself with increasing energy of incident photons. With the opening of $1s/\mathrm{SU}2l \to n'l$ channels of the $1s$-photoionization, $LL\{M, N, O\}$ Coster–Kronig transitions become possible, which form a group of lines in the energy range of 0–26 eV.

Finally, let us consider ion yield spectra (Fig. 4) produced by the cascade decays of excited states of the neon atom which arise as a result of photoionization at different energies of incident photons. As can be seen, as the energy of incident photons increases above the threshold of single K shell ionization, the relative probability of Ne^{3+} ion formation increases. Taking into account the above discussion of probabilities of formation of Ne^{q+} ions upon decays of different configurations $C_i^{(0)}$ which are created by photoionization and the behavior of photoionization cross sections (Fig. 1), this tendency becomes evident. We also note that the nonzero probability of Ne^{4+} ion formation is caused by SO processes which accompany the diagram transitions.

CONCLUSIONS

We have calculated the spectra of photons and Auger electrons and the charge spectra of ion yields which are produced by the cascade decay of excited states of the neon atom formed as a result of photoionization near the K threshold. These spectra substantially depend on the energy of incident photons. With increasing energy, channels of additional excitation/ionization processes open, which leads to a complication of spectra of emitted photons and electrons and to an increase in the yield of final ions with high charges.

Results of such calculations can be used in problems of theoretical description of the effect of ionizing radiations on meter with allowance for processes of secondary ionization of surrounding atoms by photons and electrons emitted upon cascade decays of inner vacancies [20, 29].

ACKNOWLEDGMENTS

This work was supported by the Ministry of Education and Science of the Russian Federation in terms of the federal targeted program "Research and Design in Priority Fields of the Development of the Scientific and Technological Complex of Russia in 2014–2020," agreement no. 14.607.21.0110 of November 27, 2014; unique agreement identification code RFMEFI60714X0110.

REFERENCES

1. M. O. Krause, M. L. Vestal, W. H. Johnston, and T. A. Carlson, Phys. Rev. **133**, A385 (1964).
2. T. A. Carlson and M. O. Krause, Phys. Rev. **137**, A1655 (1965).
3. M. O. Krause and T. A. Carlson, Phys. Rev. **149**, 52 (1966).
4. F. Von Busch, J. Doppelfeld, C. Gunther, and E. Hartmann, J. Phys. B **27**, 2151 (1994).
5. A. G. Kochur and V. L. Sukhorukov, J. Electron Spectrosc. Relat. Phenom. **76**, 325 (1995).
6. A. Moewes, R. G. Wilks, A. G. Kochur, and E. Z. Kurmaev, Phys. Rev. B **72**, 075129 (2005).
7. A. G. Kochur, S. Brühl, I. D. Petrov, and Y. B. Mitkina, Eur. Phys. J. Special Topics **169**, 51 (2009).
8. V. P. Sachenko and V. F. Demekhin, Sov. Phys. JETP **49** (3), 765 (1965).
9. A. G. Kochur, A. I. Dudenko, and D. Petrini, J. Phys. B **35**, 395 (2002).
10. A. G. Kochur and V. A. Popov, J. Phys. B **39**, 3335 (2006).
11. A. G. Kochur and V. A. Popov, Opt. Spectrosc. **100** (5), 645 (2006).
12. M. A. Blokhin, *Physics of X-Rays* (Gostekhizdat, Moscow, 1957) [in Russian].
13. G. B. Armen and F. P. Larkins, J. Phys. B **24**, 741 (1991).
14. S. A. Novikov, Ya. S. Akopyan, and A. G. Kochur, J. Phys. B **32**, 925 (1999).
15. A. G. Kochur, A. I. Dudenko, V. L. Sukhorukov, and I. D. Petrov, J. Phys. B **27**, 1709 (1994).
16. A. G. Kochur, V. L. Sukhorukov, A. I. Dudenko, and P. V. Demekhin, J. Phys. B **28**, 387 (1995).
17. A. G. Kochur, A. M. Nadolinsky, and V. F. Demekhin, J. Phys. Colloque **C8** (Suppl. 12), 8 (1986).
18. A. G. Kochur, A. M. Nadolinskii, and V. F. Demekhin, Opt. Spektrosk. **64** (1988).
19. R. Preseren, A. Kodre, I. Arcon, and M. Borowski, J. Synchrotron Rad. **8**, 279 (2001).
20. S. Brühl and A. G. Kochur, J. Phys. B **45**, 135003 (2012).
21. A. P. Chaynikov and A. G. Kochur, ScienceJet **4**, 91 (2015).
22. V. L. Sukhorukov, A. I. Dudenko, M. E. Vasil'eva, and A. P. Dement'ev, Izv. Akad. Nauk SSSR **55** (12), 2472 (1991).

23. A. G. Kochur, Doctoral Dissertation (Rostov-on-Don, 1997).

24. R. Kau, I. D. Petrov, V. L. Sukhorukov, and H. Hotop, Z. Phys. D **39**, 267 (1997).

25. A. B. Migdal, *Qualitative Methods in Quantum Theory* (Nauka, Moscow, 1975) [in Russian].

26. A. Migdal, J. Phys. (USSR) **4**, 449 (1941).

27. E. L. Feinberg, J. Phys. (USSR) **4** P, 423 (1941).

28. T. A. Carlson and C. W. Nestor, Phys. Rev. A **8**, 2887 (1973).

29. S. Brühl and A. G. Kochur, J. Phys. B **43**, 105002 (2010).

30. V. L. Sukhorukov, V. F. Demekhin, V. V. Timoshevskaya, and C. B. Lavrent'ev, Opt. Spektrosk. **47**, 407 (1979).

31. A. G. Kochur, V. L. Sukhorukov, and V. F. Demekhin, Relat. Phenom. **137–140**, 325 (2004).

32. B. Kanngießer, M. Jainz, S. Bruenken, W. Benten, Ch. Gerth, K. Godehusen, K. Tiedtke, P. van Kampen, A. Tutay, P. Zimmermann, V. F. Demekhin, and A. G. Kochur, Phys. Rev. A **62**, 014702 (2000).